

On the mechanism of intergranular stress corrosion cracking of sensitized stainless steel in tetrathionate solution

Akio Yonezu · Ryota Kusano · Xi Chen

Received: 4 October 2012 / Accepted: 14 November 2012 / Published online: 27 November 2012
© Springer Science+Business Media New York 2012

Abstract Intergranular stress corrosion cracking (SCC) mechanism in sensitized stainless steel (Type 304) was investigated experimentally. A tetra-thionic potassium ($K_2S_4O_6$) chemical solution was used to mimic polythionic acid SCC which the most aggressive SCC type. During the SCC test, the steel specimen was subjected to three-point bending with constant strain at room temperature, and simultaneous monitoring of acoustic emission and corrosion potential were employed to monitor SCC initiation and progression. At the early stage, transient phenomenon of local anodic dissolution was observed. Upon initiation of SCC, passivation film fracture and dissolution of metal at specimen surface take place. Through microscopic observation of SCC tip, it was found that the SCC tip advanced along the grain boundary with further mechanical loading. This suggested that the stress component plays a significant role of SCC propagation, in addition to the effect of the localized metal dissolution along Cr-depleted grain boundaries.

Introduction

Intergranular (IG) stress corrosion cracking (SCC) is one of the most commonly observed types of local corrosion damage, for sensitized stainless steel in chloride, high temperature and high pressured water and polythionic acid. Polythionic acid SCC of Type-304 steel was frequently experienced in desulfurization equipments in petro-refinery industry, where the polythionic acid is produced by oxidation of iron sulfide, and furnace tube and heat exchangers in the desulfurization process provide potential feasibility to this catastrophic disaster [1–3]. Countermeasures are recommended by the NACE standard RP 0170-2004 [4] and have been taken at every shut down maintenance. These involve, (1) shut-out of the wet atmosphere by dry air or nitrogen gas and (2) neutralization of the acid (wash by 2 % Na_2CO_3 or 1.4–2 % soda-ash solution). Indeed, the severity of the polythionic acid SCC is higher than other SCCs by chloride ion and high temperature water, which may destroy the equipment at room temperature in a day [1, 3]. The crack propagation velocity of polythionic acid SCC is very fast, faster than the macroscopic crack propagation velocity of other SCC.

Despite of its importance, studies on the polythionic acid SCC are very few and its mechanism has not been well-understood. Hosoya et al. [5] proposed a non-toxic solution (tetra-thionic potassium $K_2S_4O_6$) to simulate the polythionic SCC. Several other similar studies indicated that the tetrathionate solution produces IG-SCC at room temperature in a short period of time [6–9]. Consequently, such a tetrathionate solution has been commonly used in experiments which produces IG-SCC quickly, and enables the investigation of IG-SCC mechanism [6, 7] and the feasibility of monitoring technique [8, 9].

A. Yonezu (✉) · R. Kusano
Department of Precision Mechanics, Chuo University,
1-13-27 Kasuga, Bunkyo, Tokyo 112-8551, Japan
e-mail: yonezu@mech.chuo-u.ac.jp

X. Chen (✉)
Department of Earth and Environmental Engineering, Columbia
University, 500 W 120th Street, New York, NY 10027, USA
e-mail: xichen@columbia.edu

X. Chen
International Center for Applied Mechanics, SV Lab, School of
Aerospace, Xi'an Jiaotong University, Xi'an 710049, China

Among new techniques monitoring crack propagation in metals, one of them is the corrosion potential fluctuation (CPF), also referred to as electrochemical noise analysis [10, 11]. In CPF, a high resolution (μV) monitoring system detect the initiation of localized corrosion of metal in solution, and the non-faradic reactions due to local anodic dissolution are detected with characteristic potential fluctuations. Another monitoring technique is acoustic emission (AE), although anodic dissolution does not produce any AE. Some studies [9, 12] used AEs for mechanistic study of IG-SCC, including polythionic SCC, and reported that the AEs were produced by IG-SCC associated grain boundary separation. The reason how such fast intergranular cracking occurs was, however, not discussed. If active-path type SCC (APC-SCC) takes place in IG-SCC, it requires extremely high anodic current density of a few amperes per square centimeter. Such a high current density cannot be achieved by ohmic and diffusional resistance [13, 14].

Therefore, simultaneous monitoring of AE and CPF is expected to supply important information in the mechanistic study of SCC, and to become a powerful tool in SCC monitoring. The paper aims to bridge this gap by conducting a combined AE and CPF study of polythionic acid SCC, which will help to understand the IG-SCC mechanism as well as in situ monitoring of material and structural integrity.

Specimen and experimental setup

A solution of 0.1 mass% tetra-thionic potassium ($\text{K}_2\text{S}_4\text{O}_6$) at pH 2 is used, which was reported to cause IG-SCC at room temperature [6–8]. By controlling the amount of sulfuric acid (H_2SO_4) at 25 °C, the pH of solution was adjusted to be about 2.0—this value was reported to be useful for accelerated SCC test [8]. Specimen used in this study was Type-304 stainless steel plate of 115 mm length, 35 mm width, and 2 mm thickness, and mechanically polished to obtain smooth surface. After polishing, the specimen was fully sensitized at 650 °C for more than 24 h in vacuum. By etching with oxalic acid, it was observed that the typical grain sizes were in the range of about 30–100 μm .

Experimental setup is shown in Fig. 1. Specimens underwent three-point bending to induce a surface stress of 400 MPa ($\epsilon = 1.2\%$), and the applied strain is estimated from the radius of curvature of the specimen. As shown in Fig. 1, a glass cell with diameter of 25 mm is glued on the specimen surface, which contains the corrosive solution. AEs were monitored by four resonant type AE sensors (JT-Toshi, Type M304A, frequency band from 0.2 to 1.5 MHz) mounted on the surface of the specimen, and

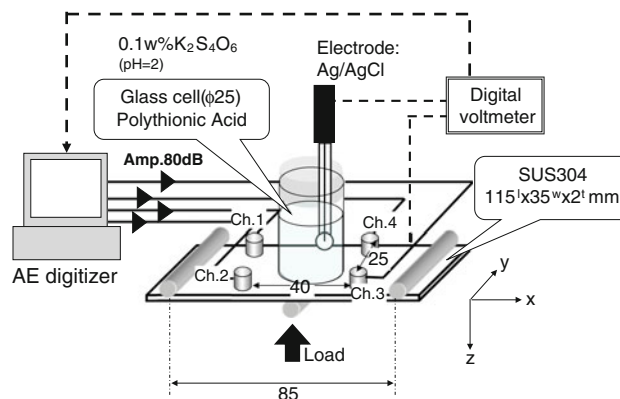


Fig. 1 Experimental setup for three-point bending SCC test integrated with simultaneous damage monitoring technique of acoustic emission and corrosion potential fluctuation

amplified to 80 dB by preamplifiers, digitized by an A/D converter and fed to a personal computer. The corrosion potential was monitored by a Ag/AgCl reference electrode immersed in the solution, and digitized by a digital voltmeter (ADVANTEST, RE6871E) and fed to the same personal computer. The vertical resolution of the volt meter is 0.1 μV and sampling interval is 0.25 s.

Experimental results and discussion

Potential fluctuation and AE

Since the polythionic SCC is significantly influenced by corrosion potential, the timing of corrosion potential and AE generation was studied. Figure 2 compares the changes in corrosion potential and cumulative AE hit counts with test time. To evaluate the AE signals amplitude, the root mean square value (i.e., AE energy) is calculated and plotted as shown by gray symbols. Here, it is noted that the equilibrium potential of Ag/AgCl electrode is +225 mV versus normal hydrogen electrode (N.H.E). The corrosion

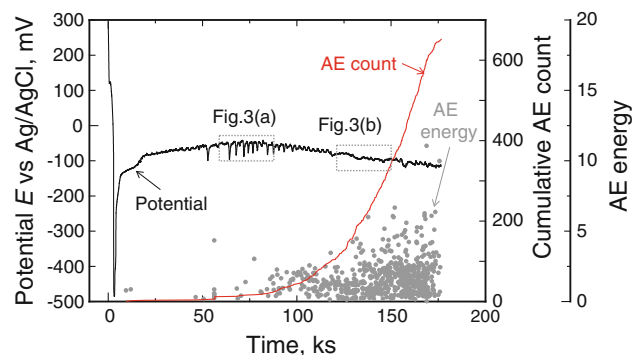


Fig. 2 Changes in corrosion potential fluctuation, cumulative AE count and AE energy

potential shifts quickly to active potential of -500 mV versus Ag/AgCl (-275 mV vs. N.H.E.) and recovers to -100 mV ($+125$ mV vs. N.H.E.) at the beginning of the test. It was observed that the specimen surface is covered by black film within 20 ks.

After 50 ks, potential fluctuation is frequently observed. Figure 3a shows the magnified view of the range from 60 to 90 ks in Fig. 2. The potential shows a characteristic fluctuating signal, exhibiting rapid drop and recovery; this is the RD-type CPF. These signals are caused by non-faradic reaction due to local anodic dissolution, such as pitting and IG corrosion (grain boundary attack). Therefore, RD-type CPF signals are often recognized as coming from SCC initiation, and thus are very useful to identify the timing of SCC initiation. As shown in Fig. 3a, strong amplitude of the CPFs was observed in the time range of 50–100 ks. However, the frequent RD-type CPFs gradually decreased. In fact, as shown in Fig. 3b, the amplitude of fluctuation is smaller than that of Fig. 3a. At this stage (after about 100 ks), however, the AE counts were rapidly increased, and finally reached to the cumulative AE counts

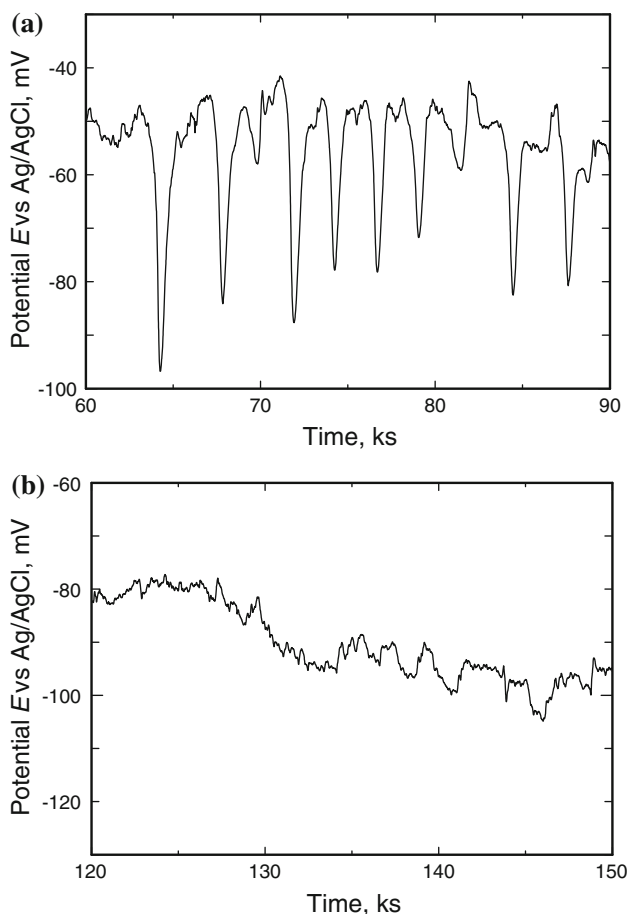


Fig. 3 Enlarged period of test time in Fig. 2: **a** 60–90 ks and **b** 120–150 ks

of 600 events. In addition, their AE energy became larger with the increase of AE count. In fact, at 150 ks, SCC was observed by eye inspection during the test.

In general, AE is produced by the release of elastic strain energy when small fracture occurs due to mechanical loading. On the other hand, dissolved metal does not produce any AE. As shown in Fig. 2, the SCC test produced both AE and CPF. Their timing yield useful information on SCC initiation and progression and the role of mechanical loading, influencing SCC. The detailed investigation is described later.

Crack morphology

After SCC with about 5 mm long crack was clearly observed, the SCC test was stopped (at about 180 ks, see Fig. 2). The specimen was washed with ethanol and purified water by ultrasonic washing machine, so that the corrosive solution in the crack propagation path of SCC was removed. A typical example of crack morphology is shown in Fig. 4. We observed very clear IG-SCC in Fig. 4a, which is the main SCC that propagates perpendicular to the direction of the maximum tensile stress. Around this crack, many grain boundary defects (grain boundary dissolution) were also observed. In addition, scanning electron microscope was used to observe the main IG-SCC as shown in Fig. 4b and c, exhibiting clear IG cracking. This morphology is often observed in polythionic acid SCC [1, 3]. Furthermore, hydrogen embrittlement produces similar morphology [15]. If such a crack was caused by anodic dissolution of metal (i.e., Cr-depleted zone at grain boundary), it should not produce any AEs. However, if there is contribution of mechanical separation against grain boundary, it possibly produces AEs as what has been observed in the present study.

Referring to Fig. 2, the corrosion potential from anodic dissolution was observed first. Subsequently numerous AEs were detected when SCC is observed. Thus, it is expected that the SCC progression is contributed by mechanical loading. In order to investigate how the tensile stress affects SCC progression, the specimen after SCC test was further applied with mechanical loading.

Bending test for specimen with SCC

After the SCC test, the specimen was cut for bending test in atmosphere. One cut line was across the main SCC to observe the depth of SCC. The length, width, and thickness of the cut specimen are about 50, 8.5, and 2 mm, respectively. A hydraulic tester (Shimadzu Corp, EHF-1) is used for four-point bending test, where the inner span is 10 mm and outer span is 30 mm. The position of main SCC was set in inner span. The load was gradually applied with the

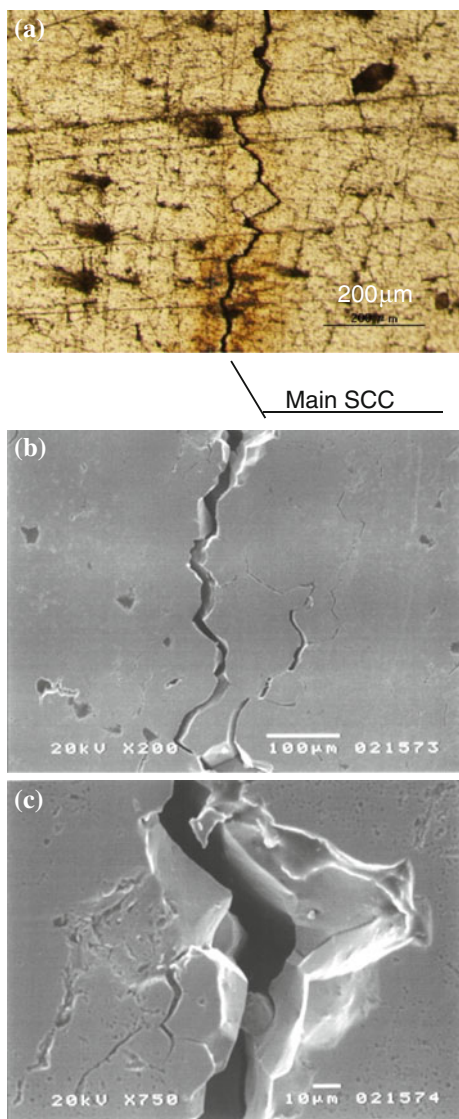


Fig. 4 Micrographs of IG-SCC taken by optical microscope (a) and scanning electron microscope (SEM) (b, c). c Magnified area in (b)

displacement control. Two AE sensors were mounted on the specimen surface to monitor the generation of small crack during the test. Figure 5 shows the transverse section around the main SCC using SEM. Before the bending test, the depth of SCC was about 0.7 mm, while the crack tip progressed to be 1.2 mm after the test. Figure 6a shows the relationship between the load and displacement. This figure also plots the cumulative AE count as indicated by dashed line. Among them, the large AE associated with Mode I fracture is plotted by triangle marks. The result showed that the load increases linearly up to 30 N. After that, the load suddenly decreased and showed constant value. At this point, the number of AE is rapidly increased and several large AEs were also detected. In fact, AE sources were identified by difference of traveling velocity among the two

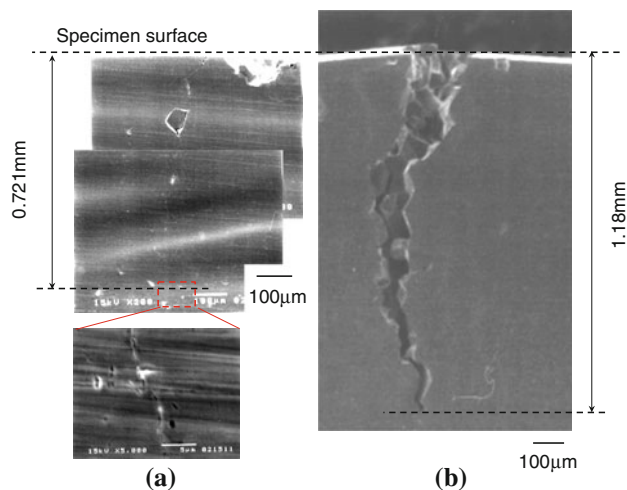


Fig. 5 SEM photos of IG-SCC observed from side surface in the specimen for four-point bending test. The left photo is before bending test and the right one is after the test, showing crack significantly advances

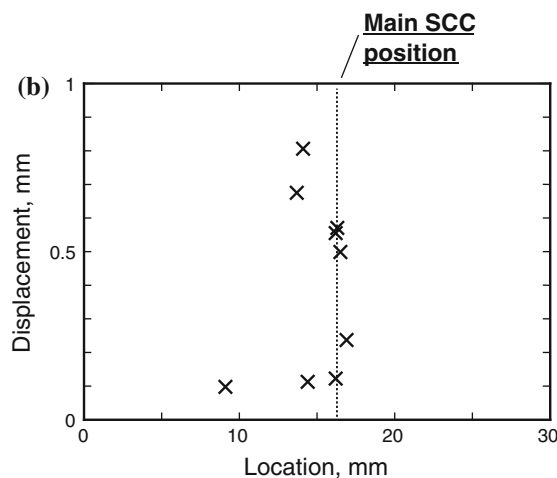
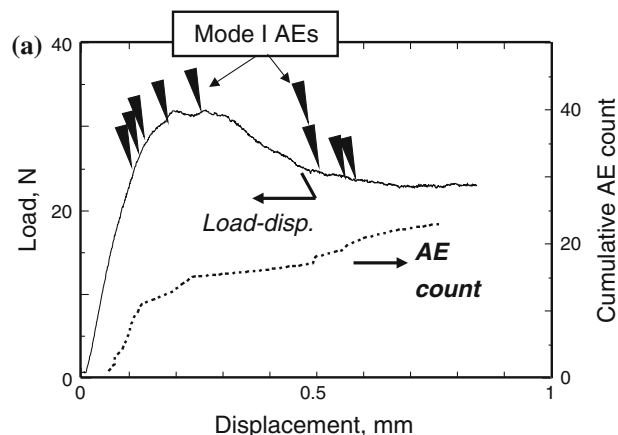


Fig. 6 Load-displacement curve of SUS304 with SCC subjected to four-point bending (a). a The timing of AE generation and cumulative AE count. b Source location of AEs detected during four-point bending

Fig. 7 Snapshot of microscopic picture of IG-SCC path at the applied bending strain of 1.1, 1.4, and 1.6 %

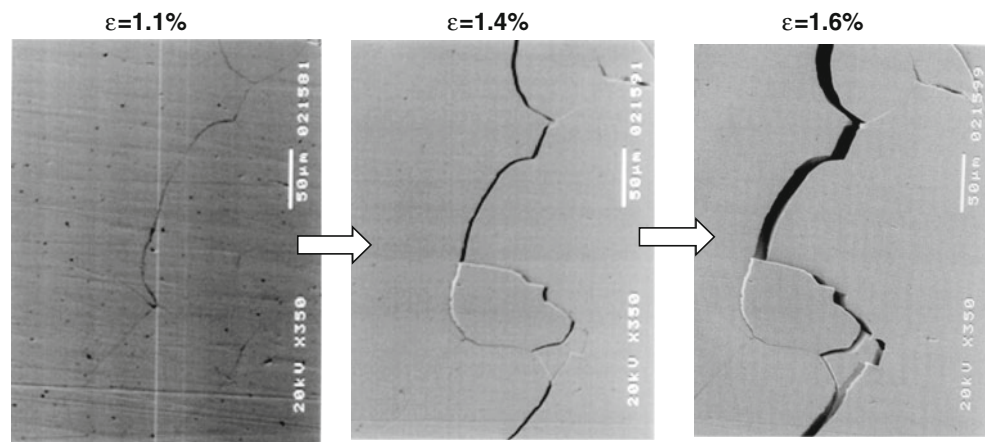
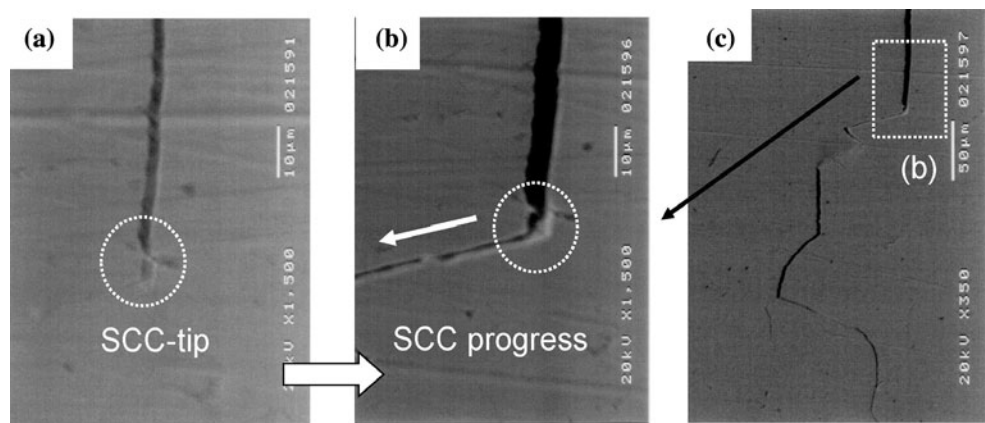


Fig. 8 SEM picture around SCC tip. **a** The tip at strain of 1.4 % and **b, c** the crack path at 1.6 % strain



AE channels, indicating that AEs were located on main SCC position (see Fig. 6b). These results thus suggested that the tip of SCC advanced due to purely mechanical loading using four-point bending test. It also suggested that crack progression emit many AEs.

To clarify how the crack propagates along the grain boundary, microscopic observation was conducted using SEM. As mentioned above, the specimen with SCC was cut for mechanical test. One side was used for the four point bent test with AE (see Fig. 5). Another specimen with SCC was used in this experiment. The jig of three-point bent for SCC test (see Fig. 2) was again used as mechanical loading. Since the SCC test was conducted at 1.2 % strain, bending strain was increased up to 1.6 %. The snapshot of microscopic picture was taken by SEM, when the applied strain was 1.1, 1.4, and 1.6 %.

Figure 7 shows the picture of representative crack path with low magnitude. Until the strain of 1.1 %, very fine crack was observed. With increasing strain, the crack path was clearly observed, namely the crack opening displacement becomes wider. Figure 8a shows the crack tip of SCC at the strain of 1.1 %. However, at strain of 1.4 %, the crack was found to advance along the grain boundary as

shown in Fig. 8b. The surrounding area shown in Fig. 8c suggests that the crack advanced with several hundred μm along the grain boundary. In addition, other crack tip is observed as shown in Fig. 9a (at the strain of 1.4 %). After applying strain up to 1.6 %, the crack propagates again as shown in Fig. 9b. Note that after the SCC test, the specimen was washed with ethanol and purified water by ultrasonic washing machine, so that it is expected that the corrosive solution (anion species) was minimized (or very little) in the crack propagation path of SCC. Thus, it is revealed that mechanical loading plays an important role of SCC progression, accelerating SCC propagation.

Effect of stress on SCC progression

By referring the above-experimental results the mechanism of IG-SCC, in particular crack growth, is summarized as follows. Figure 10 shows the schematic mechanism of grain boundary separation and IG-SCC. First, the depleted zone is attacked by the anodic dissolution, and the attacked grains are mechanically exfoliated by the tensile stresses. This is due to the fact that (see Fig. 2) the CPF (from local anodic dissolution) was first detected, and subsequently AE

Fig. 9 Snapshot of microscopic picture of IG-SCC path at the applied bending strain of 1.4 (a) and 1.6 % (b). This area is different from that in Figs. 7 and 8

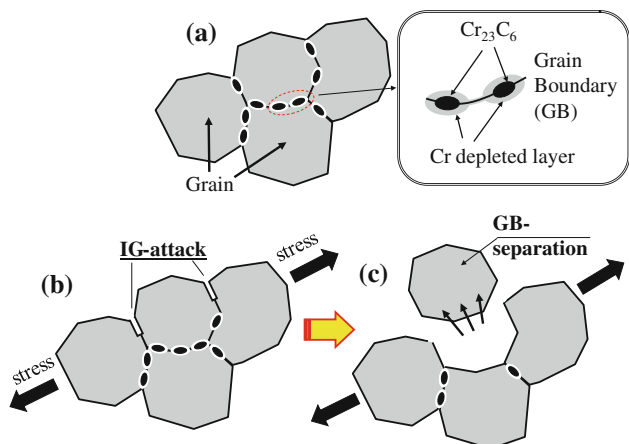
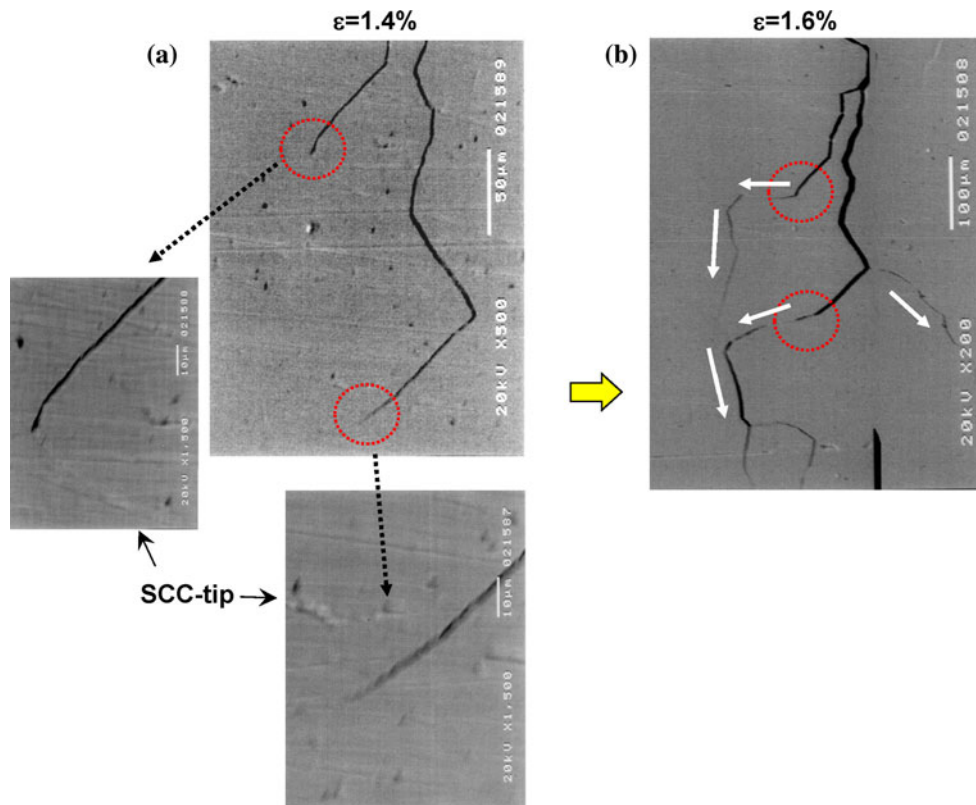


Fig. 10 Schematic of proposed mechanism of initiation and progression of IG-SCC. **a** Cr-depleted layer develops at grain boundary due to sensitization. **b** Grain boundary attack occurs due to local anodic dissolution, producing RD-CPF. **c** Grain boundary separation (intergranular cracking) produces due to stress concentration around IG-attack

(from mechanical fracture) was produced. The number of AE and their amplitude increased when the testing time was longer.

After grain boundary dissolution (referred to as the IG-attack), stress concentration takes place at the tip of grain boundary. The concentration encourages the grain boundary separation due to large tensile stresses, which

produces AE. This can be confirmed from the experimental evidence (e.g., “Bending test for specimen with SCC” section shows that the IG crack advanced when mechanical loading was applied on the IG-SCC specimen). Such a crack propagation process produces AEs (Fig. 6) and it was very similar to the IG-SCC morphology (Figs. 8, 9).

It can be summarized that the IG cracking is attributed to the synergistic interaction of electrochemical and mechanical actions. Besides, the tensile stress accelerates the grain boundary separation, possibly due to the grain boundary decohesion stresses. The decohesion strength may be decreased owing to volume reduction by anodic dissolution or hydrogen embrittlement. Indeed, previous studies reported that hydrogen embrittlement of austenitic stainless steel showed clear IG cracking and produced many AEs [15]. Although in the present study the role of hydrogen embrittlement to IG-SCC propagation remains unclear, the decohesion strength of grain boundary and separation due to mechanical loading is found to dominate the IG-SCC mechanism.

Conclusion

One of the famous SCC types, the IG stress corrosion cracking (IG-SCC), is mainly produced by grain boundary dissolution (IG-attack) due to electrochemical action. This

study aims to investigate the mechanism of IG-SCC in sensitized stainless steel (Type 304), in particular how mechanical loading affects IG-SCC. A tetra-thionic potassium ($K_2S_4O_6$) chemical solution was used to produce IG-SCC at room temperature. During the SCC test, simultaneous monitoring of AE and CPF were employed to monitor SCC initiation and progression. In the early stage, many RD-type CPF signals (from transient phenomena of local anodic dissolution) were observed, indicating the initiation of SCC, i.e., passivation film fracture and dissolved metal at specimen surface took place. Subsequently, many AEs were detected and their amplitude and the number increased with testing time. It can hypothesize that these AEs were produced by mechanical fracture (not anodic dissolution). Thus, the present IG-SCC behavior is attributed to the synergistic interaction of electrochemical and mechanical actions. In order to clarify the role of mechanical loading to IG-SCC, microscopic observation by scanning electron microscope was employed to observe the SCC tip behavior when mechanical loading was applied. It was found that the SCC tip advanced along the grain boundary with further mechanical loading. This suggested that the stress component plays a significant role during SCC propagation, in addition to the effect of the localized metal dissolution along Cr-depleted grain boundaries. The study also verified that the simultaneous monitoring of AE and CPF may supply important information in the mechanistic study of SCC, and thus it is a useful approach in SCC monitoring.

Acknowledgements We would like to thank Professor Mikio Tekemoto (Aoyama Gakuin University, Kanmeta Engineering Co., Ltd.) for his guidance. The work of A.Y. is supported in part of Grant-in-Aid for Young Scientist of (B) (No. 22760077) of the Ministry of

Education, Culture, Sports, Science and Technology, Japan, and Research Grant for Science and Technology of SUZUKI Foundation. The work of X.C. is supported by the National Natural Science Foundation of China (11172231), the World Class University program through the National Research Foundation of Korea (R32-2008-000-20042-0), and the National Science Foundation (CMMI-0643726).

References

1. Nishida H, Nakamura K, Takahashi T (1984) *Mater Perform* 23:38
2. Kowaka M, Kudo T (1979) *J Jpn Inst Met* 43:595
3. Ahmad S, Mehta ML, Saraf SK, Saraswat IP (1981) *Corros NACE* 37:412
4. NACE (2004) Protection of austenitic stainless steel and other austenitic alloys from polythionic acid stress corrosion cracking during shutdown of refinery equipment NACE standard recommended practice. RP0170-2004
5. Hosoya K, Yamamoto K, Kagawa N (1985) *Boshoku-Gijyutu* 34:568 (in Japanese)
6. Rahimi S, Engelberg DL, Duff JA, Marrow TJ (2009) *J Microsc Oxf* 233:423
7. Marrow TJ, Babout L, Jivkov AP, Wood P, Engelberg D, Stevens N, Withers PJ, Newman RC (2006) *J Nucl Mater* 352:62
8. Breimesser M, Ritter S, Seifert H-P, Suter T, Virtanen S (2012) *Corros Sci* 45:1747
9. Takemoto M, Nakazawa T (1995) *Boshoku-Gijyutu* 44:166 (in Japanese)
10. Inoue H (2003) *Corros Eng* 52:444
11. Inoue H, Iwakawa H, Yamakawa K (1995) *Mater Sci Eng A* 198:225
12. Yonezu A, Cho H, Takemoto M (2006) *Prog Acoust Emission* III:489
13. Kelly RG, Frost AJ, Shahrabi T, Newman RC (1991) *Metall Trans A* 22:531
14. Yonezu A, Cho H, Takemoto M (2006) *Meas Sci Technol* 17:2447
15. Carpenter SH, Amith DR (1990) *Metall Trans A* 21:1933